

Thermal Neutron Scattering Data Revision for Graphite and Beryllium

M. EL BARBARI^{a,*}, T. EL BARDOUNI^a, H. ZIANI^a,
H. EL YAAKOUBI^a, A. EL MTILI^a,
Y. BOULAICH^b AND C. EL YOUNOUSSI^b

^aLaboratory of Radiations and Nuclear Systems, Faculty of Sciences,
Abdelmalek Essaadi University, Tetouan, Morocco

^bNational Center for Energy Sciences and Nuclear Techniques, Rabat, Morocco

Received: 01.10.2020 & Accepted: 24.12.2020

Doi: [10.12693/APhysPolA.139.118](https://doi.org/10.12693/APhysPolA.139.118)

*e-mail: moniaelbarbari@yahoo.fr

Keeping nuclear data libraries updated is crucial for securing nuclear facilities. This study contributes to the progress made in the first-principles calculations and advancement in computational materials. Specifically, this paper describes the *ab initio* derivation of vibrational properties of two important materials used in nuclear facilities (graphite and beryllium) and evaluates neutron scattering cross-sections and heat transport. To this end, a study was performed with the ABINIT code package, using the carefully described structure of graphite and beryllium. Phonon spectra which affect the thermal scattering law were identified and neutron scattering cross-sections calculations were performed. The important neutron and heat transport functions were derived with the LEAPR and THERMR modules of NJOY code.

topics: ABINIT, phonons, NJOY, graphite

1. Introduction

Graphite and beryllium — due to their low atomic weights, low neutron absorption cross-sections and high neutron scattering cross-sections — are successfully used in nuclear reactors as moderators, reflectors or even filters. Furthermore, their high strength at elevated temperatures, high sublimation point and resistance to rupture by thermally induced stress make them the materials of choice in nuclear technology [1].

This study describes the phonon dispersion spectra, scattering law $S(\alpha, \beta)$ and the coherent, incoherent and total thermal neutron scattering cross-sections for graphite and beryllium. The *ab initio* calculation method was used, as well as two approximations: local density approximation (LDA) for a typical study of graphite and beryllium and generalized gradient approximation (GGA) in the case of graphite. The effects of Van der Waals bonding in a crystal were considered [2, 3].

2. Method and computational details

First, we precisely describe the crystal structure of the studied material. This description includes the lattice parameters, the atoms position, the unit and supercell characteristics and the k -mesh for the Brillouin zone (BZ) sampling. Afterwards,

the first-principles (*ab initio*) calculations were performed and two main approximations, LDA and GGA, were used. LDA assumes that the exchange-correlation energy functional is local and the contribution at each point is independent of other points to simplify the calculations [4]. This approximation is used in the case of graphite without the Van der Waals contribution and for beryllium. GGA assumes that the exchange-correlation contribution depends both on the magnitude of the electronic density and its gradient [5]. For reasons of compatibility between this approximation and the Van der Waals exchange-correlation options available in ABINIT code, we opted to use it in the second case of graphite. Based on these assumptions, the phonon spectra are computed for both graphite and beryllium.

The most important thermal properties which derive from the phonon density of states (DOS) are the heat capacity given by

$$T_{\text{eff}} = \frac{1}{2} \int_0^{\omega_{\text{max}}} \hbar \omega \rho(\omega) \coth\left(\frac{\omega}{2k_{\text{B}}T}\right) d\omega, \quad (1)$$

the effective scattering temperature used by the LEAPR module in the generation of the thermal scattering law data and given by

$$\gamma(0) = \int_0^{\omega_{\text{max}}} \frac{\rho(\omega)}{\hbar \omega} \coth\left(\frac{\omega}{2k_{\text{B}}T}\right) d\omega, \quad (2)$$

and also the Debye–Waller integral of the form

$$\frac{C_v}{3R} = \int_0^{\omega_{\max}} \rho(\omega) \frac{\omega}{k_B T} \frac{e^{\omega/k_B T}}{(e^{\omega/k_B T} - 1)^2} d\omega, \quad (3)$$

which is needed for calculating the elastic coherent and the incoherent neutron scattering cross-sections. Here, R is the gas constant, ω — the frequency, k_B — the Boltzman constant and T is the temperature. These parameters are processed by the LEAPR module of NJOY to generate the thermal scattering law $S(\alpha, \beta)$ which will be used by the THERMR module to calculate the scattering cross-sections.

3. Results and discussion

3.1. Atomic and electronic structure

Graphite has a lamellar or quasi-two-dimensional structure belonging to the space group $P6_3/mmc$ (194). The bonding in graphite exhibits one of the largest anisotropies of any solid. The nearest-neighbor bond in graphite is considered stronger than the nearest neighbor bond in diamond. This strong bond is a covalent sp^2 (σ -bond) and has a short length of 2.45 Å. In contrast, the bonding between planes is very weak and exhibits Van der Waals interaction. The spacing between layers is relatively large (6.70 Å) and the ratio $c/a = 2.73$. Since beryllium atoms have the electronic configuration $2s^2$ with a hexagonal close-packed structure, consequently beryllium belongs to the same space group $P6_3/mmc$ with the lattice parameters: $a = b = 2.2866$ Å, $c = 3.5833$ Å and $c/a = 1.57$.

The exact crystal parameters, obtained by the assignment of the Wyckoff positions using Bilbao Crystallographic Server data [6], are presented in Table I.

The most common and abundant stacking sequence of the graphite crystal is the hexagonal (α - or Bernal) structure with a -ABAB- stacking order presented in Fig. 1a. Almost 85% of natural graphite has this stacking [7]. The unit cell of graphite contains 4 carbon atoms ($2 + 8 \times \frac{1}{4} = 4$), two in each layer. For beryllium, the unit cell is composed of 2 atoms ($1 + 8 \times \frac{1}{8} = 2$), as shown in Fig. 1b.

TABLE I

Wyckoff positions of carbon atoms in graphite.

Atom	Wyckoff letter	Site symmetry	Atomic orbit
C1 (graphite)	b	$-6m2$	$(0, 0, \frac{1}{4})$, $(0, 0, \frac{3}{4})$
C2 (graphite)	c	$-6m2$	$(\frac{1}{3}, \frac{2}{3}, \frac{1}{4})$, $(\frac{2}{3}, \frac{1}{3}, \frac{3}{4})$
B1 (beryllium)	a	$-3m$	$(0, 0, 0)$
B2 (beryllium)	f	$3m$	$(\frac{1}{3}, \frac{2}{3}, \frac{1}{2})$

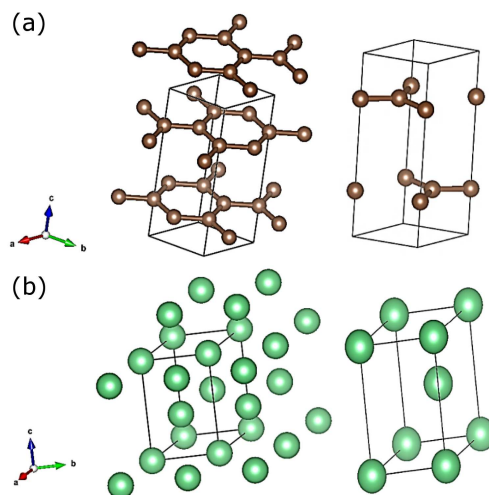


Fig. 1. The hexagonal packed structure (left) and the unit cell (right), for graphite (a) and beryllium (b).

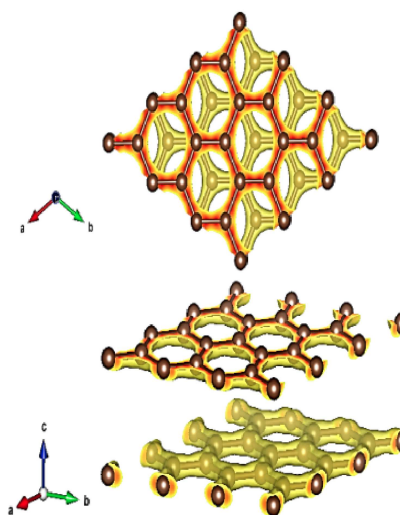


Fig. 2. The density of charges in graphite following the 110 and 001 plans; from low probability (yellow) to high probability (red).

VESTA visualization software, which is a 3D specialized program for structural models and electron densities [8], was used in this work to produce structural geometries.

The graphite charges density is mostly condensed in the interspatial plan as presented in Fig. 2. As the density becomes higher in the covalent bond, other phenomena also emerge with significant probabilities such as the thermal and electric conductivity or vibrational modes. In the Van der Waals bond, in turn, these phenomena are almost absent. Thus, it is perfectly normal not to consider the vibrational effects of graphite in the study of phonon modes for nuclear applications. Therefore, considering the two cases mentioned above, we investigate the impact of the phonon modes associated with each of them on the total neutron scattering cross-sections.

3.2. Phonon spectra

The *ab initio* calculations were performed using ABINIT code. It allows to do lattice parameter optimization, calculations of force constants and density of states. For graphite, a $6 \times 6 \times 3$ supercell (432 atoms) was used in both cases. The obtained phonon spectrum shows two kinds of differences (see Fig. 3): (i) the magnitude of peaks is clearly higher for GGA+VDW calculations due to the addition of phonon densities from the Van der Waals bond and (ii) the shifting of some peaks.

While the acoustic shear (SH), longitudinal acoustic (LA), optical shear (SH*) and longitudinal optical (LO) branches are practically superposed, the branches of out-of-plane acoustic (ZA) and out-of-plane optical (ZO) branches show some deviation. This discrepancy is essentially caused by the differences between LDA and GGA approximations, on which the *ab initio* calculations are based. Table II presents comparative results between our calculations and experimental data obtained by Vitali et al. [9].

A general comparison does not allow to distinguish the best case to choose, since the two methods accord with the experimental results in the majority of modes and slightly diverge in others. Nevertheless, slight differences in the calculation methods can cause significant differences in the resulting phonon spectra. Figure 4 clearly shows such differences between our spectra and those of ORNL [10], NCSU [11] and General Atomics (GA) [12], as published by the International Nuclear Data Committee (INDC) [13].

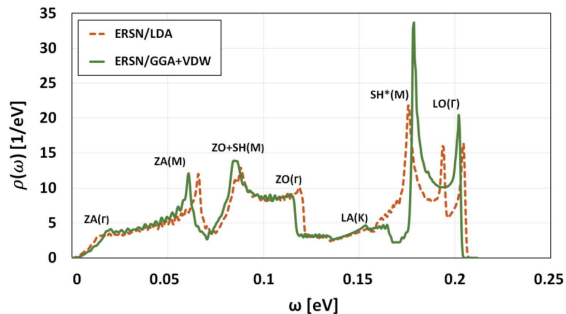


Fig. 3. Graphite phonon frequency distributions.

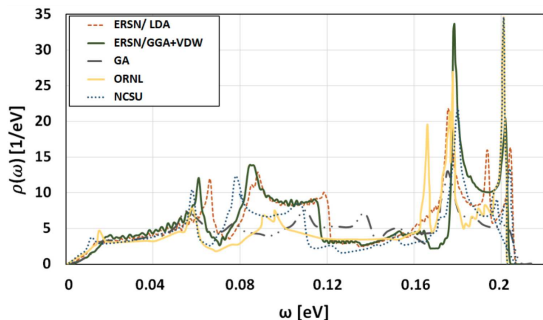


Fig. 4. Graphite phonon frequency distribution compared to GA, ORNL and NCSU.

TABLE II

Phonon branches compared to experimental results in [eV] units.

Phonon branches	ERSN		Exp. [9]
	LDA	GGA+VDW	
ZA (Γ)	0.016	0.019	0.016
ZA (M)	0.066	0.060	0.058
ZO+SH(M)	0.082–0.087	0.085–0.086	0.081–0.1
ZO (Γ)	0.118	0.114	0.111
SH*(M)	0.177	0.178	0.180
LO (Γ)	0.202	0.201	0.200

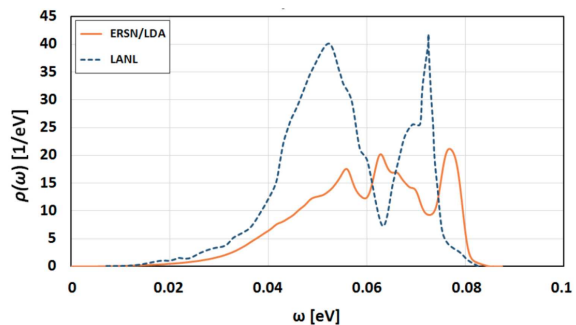


Fig. 5. Beryllium phonon frequency distribution.

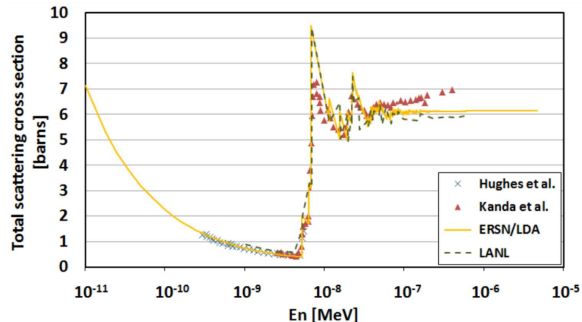


Fig. 6. Total neutron scattering cross-section for beryllium at 293 K.

Regarding the beryllium phonon spectrum, the dispersion relations were calculated using the local density approximation LDA only. In this example, a $4 \times 4 \times 4$ supercell (128 atoms) was considered. Similarly, $4 \times 4 \times 4$ k -mesh points were generated by the Monkhorst and Pack scheme over the Brillouin zone. Beryllium is a polycrystalline metal, thus the phonon distribution is a continuous spectrum, as it is shown in Fig. 5.

The phonon spectrum obtained by the LDA method differs from that obtained by R.E. MacFarlane (Los Alamos National Laboratory — LANL) [14], however, the neutrons scattering cross-sections (see Fig. 6) demonstrate a clear improvement when using the ERSN phonon DOS in comparison with the one obtained by LANL.

TABLE III

 Effective scattering temperature T_{eff} and Debye–Waller integral $\gamma(0)$ for graphite and beryllium at 293 K.

	ERSN		GA	ORNL	NCSU	LANL
	LDA	GGA+VDW				
T_{eff} [K] (graphite)	734.43	731.55	713.72	775.15	723.17	714.3
$\gamma(0)$ [eV^{-1}] (graphite)	26.09	21.27	26.9	30.48	37.58	26.17
T_{eff} [K] (beryllium)	421.42	–	–	–	–	405.9
$\gamma(0)$ [eV^{-1}] (beryllium)	25.11	–	–	–	–	28.69

3.3. Effective scattering temperature and Debye–Waller integral

The effective scattering temperature and the Debye–Waller integral are parameters correlated to the phonon spectrum and used by the THERMR module of NJOY code to evaluate the thermal neutron scattering law $S(\alpha, \beta)$ (see (1) and (2)). These parameters calculated by LEAPR are compared to those obtained by GA, ORNL, NCSU and LANL (Table III).

Regarding the graphite effective scattering temperatures, the values obtained in our results are in good agreement with those found in published works, with the exception of a slightly higher temperature published by ORNL. In the case of the Debye–Waller integral, our results remain very close to those obtained by GA and LANL, whereas NCSU values are exceptionally higher. We also noticed that adding the Van der Waals effect slightly reduces the effective temperature and the Debye–Waller integral. Regarding beryllium, only few results exist in the literature regarding the effective temperature and the Debye–Waller integral, meanwhile our results remain in good agreement with those of LANL.

The effective scattering temperatures are affected by higher frequencies (although below 0.20 eV). This explains the good agreement with the NCSU values. In fact, our two phonon DOS spectra and their phonon spectrum are very close in this domain of frequencies. While the Debye–Waller integrals are affected by lower frequencies (under 0.05 eV), our spectra are closer to general atomic phonon DOS, given similar results for the Debye–Waller integrals. Similar results were obtained for beryllium.

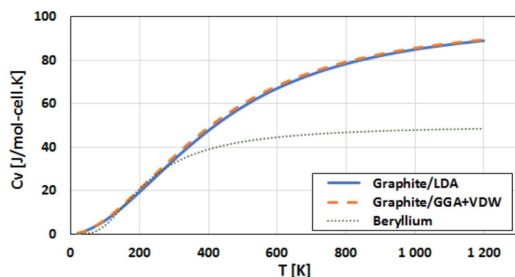


Fig. 7. Heat capacity calculated by ABINIT code for graphite and beryllium.

In fact, we find some differences with the results obtained by R.E. MacFarlane. These results are specifically due to the difference in the phonon values used to regulate these parameters.

3.4. Heat capacity and effective temperature

The heat capacity, important in determining the heat transport in materials, is calculated by ABINIT (3). Figure 7 shows that the graphite corresponding curves in the two approximations accord perfectly. Since both the thermal and electrical charge transport are associated with the covalent bond for graphite, the heat capacity is slightly affected or almost independent of the Van der Waals bonds. Comparison of the heat capacity results for graphite and beryllium revealed important differences. It is higher for graphite than for beryllium for almost all temperatures, except in the range of 180–240 K, consistent with the well-known good thermal conductivity of graphite.

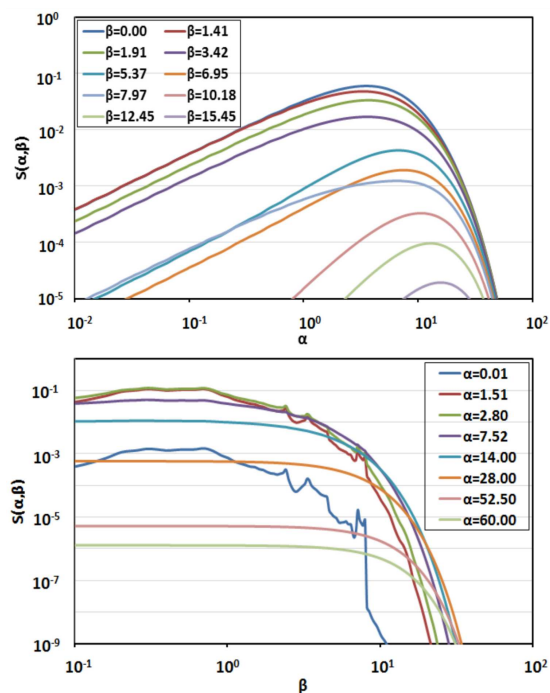


Fig. 8. Thermal neutron scattering law for graphite at 293.6 K.

3.5. Thermal scattering law $S(\alpha, \beta)$

The LEAPR module of NJOY requires a discrete grid of values of vibrational densities of states. Hence, the phonon spectra are arranged adequately to be treated in such a form. The thermal scattering laws obtained for several values of momentum transfer α and energy transfer β for both graphite and beryllium are presented in Figs. 8 and 9.

The two cases of graphite show no notable differences (almost superposed in all points). Thus, we opted to present the one with the case where the Van der Waals is taken into consideration.

3.6. Neutron scattering cross-sections

The thermal scattering law $S(\alpha, \beta)$ obtained by the LEAPR module is processed by the THERMR module of NJOY to provide separate results of the elastic coherent, inelastic incoherent and the total scattering cross-sections.

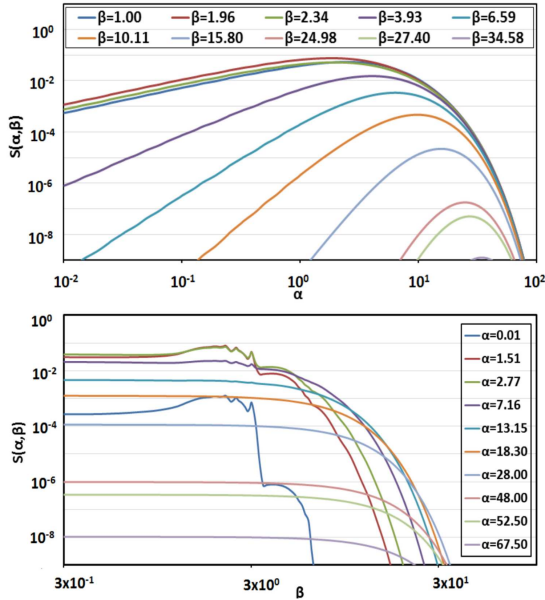


Fig. 9. Thermal neutron scattering law for beryllium at 293.6 K.

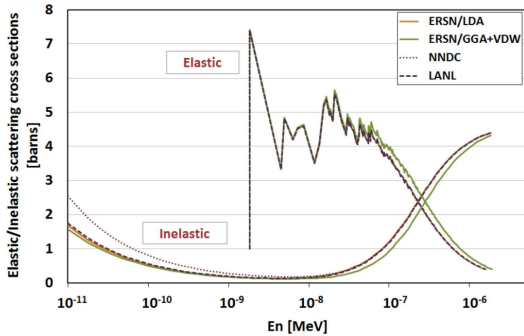


Fig. 10. Inelastic and coherent elastic neutron scattering cross-sections for graphite at 293 K.

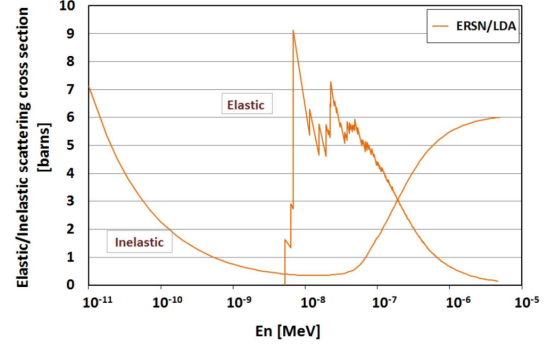


Fig. 11. Inelastic and coherent elastic neutron scattering cross-sections for beryllium at 293 K.

The obtained results for graphite elastic and inelastic scattering cross-section in LDA approximation (Fig. 10) are in good agreement with those obtained by LANL [15] and the National Nuclear Data Center (NNDC) [16] for intermediate and high energies. In the case of lower energies, the inelastic scattering cross-sections published by LANL are higher than ours and those of NNDC.

As expected, the Van der Waals effect exhibits some differences at high energies, thus the addition of this bound, which was neglected for a long time, indeed affects the elastic and inelastic scattering cross-sections.

For the beryllium case, Fig. 11 shows the inelastic and coherent elastic neutron scattering cross-sections for beryllium at room temperature, while Fig. 6 gives the total neutron scattering cross-section for beryllium at the same temperature.

The total scattering cross-sections obtained in this work (ERSN) using the local density approximation show a good agreement with LANL results and the experimental results [17, 18], which validates the method used in this study for obtaining the total neutron cross-section.

4. Conclusion

It has recently become crucial to improve and review the nuclear data libraries in view of the advancement made in the *ab initio* calculations of the phonon spectra which are necessary for the thermal neutron scattering law parameters determination. In this work, graphite and beryllium, two materials largely used in nuclear reactors, were reviewed. In graphite, the Van der Waals bonding was taken into consideration as it shows significant influence on the scattering cross-sections behavior. The two approximations (LDA and GGA) demonstrate satisfactory thermal and vibrational responses which are in accordance with the experimental data published in the literature. In the case of beryllium, the improvement of the total neutron scattering cross-section was notably achieved using the LDA approximation. In future, similar studies should apply *ab initio* procedures to prospective novel materials such as high-entropy alloys.

Acknowledgments

The authors are grateful to Ms. Bouchra Rahim of CNRST for her kind help in running ABINIT in the HPC-MARWAN cluster.

References

- [1] C.L. Mantell, *Carbon and Graphite Handbook*, 1968.
- [2] J. Wormald, A.I. Hawari, *EPJ Web of Conferences* **146**, 13002 (2017).
- [3] M. Birowska, K. Milowska, J. Majewski, *Acta Phys. Pol. A* **120**, 845 (2011).
- [4] J.P. Perdew, A. Zunger, *Phys. Rev. B* **23**, 5048 (1981).
- [5] W. Koch, M.C. Holthausen, M. Kaupp, *Angew. Chem.–German Edition* **113**, 989 (2001).
- [6] M.I. Aroyo, J.M. Perez-Mato, C. Capillas, E. Kroumova, S. Ivantchev, G. Madariaga, A. Kirov, H. Wondratschek, *Z. Kristallogr.–Cryst. Mater.* **221**, 15 (2006).
- [7] K. Myhro, S. Che, Y. Shi, Y. Lee, K. Thilalar, K. Bleich, D. Smirnov, C. Lau, *2D Mater.* **5**, 045013 (2018).
- [8] K. Momma, F. Izumi, *J. Appl. Crystallogr.* **44**, 1272 (2011).
- [9] L. Vitali, M. Schneider, K. Kern, L. Wirtz, A. Rubio, *Phys. Rev. B* **69**, 121414 (2004).
- [10] F.C. Difilippo, J.P. Renier, A.I. Hawari, “Benchmarks for the Scattering Kernel of Graphite”, in: *Proc. PHYSOR*, 2002, p. 7.
- [11] A. Hawari, I. Al-Qasir, V. Gillette, B. Wehring, T. Zhou, “*Ab Initio* Generation of Thermal Neutron Scattering Cross-Sections”, in: *Proc. PHYSOR*, 2004, p. 25.
- [12] J. Koppel, D. Houston, *Reference Manual for ENDF Thermal Neutron Scattering Data. Technical Report*, Gulf General Atomic, San Diego (CA) 1968.
- [13] M. Mattes, J. Keinert, *Status of Thermal Neutron Scattering Data for Graphite. Technical Report*, International Atomic Energy Agency, 2005.
- [14] R. MacFarlane, D. Muir, *The NJOY Nuclear Data Processing System, Version 91. Technical Report, LA-12740-M Technical Report of Los Alamos National Laboratory*, Los Alamos 1994.
- [15] P. Lisowski, C. Bowman, G. Russell, S. Wender, *Nucl. Sci. Eng.* **106**, 208 (1990)
- [16] D.A. Brown, M. Chadwick, R. Capote et al., *Nucl. Data Sheets* **148**, 1 (2018).
- [17] K. Kanda, H. Kadotani, O. Aizawa, *J. Nucl. Sci. Technol.* **12**, 601 (1975).
- [18] D.J. Hughes, R.B. Schwartz, *Neutron Cross Sections, USAEC Report BNL-325*, 2nd ed., Brookhaven National Laboratory, 1958.